Multitone FSK Modulation for SWIPT

Steven Claessens, *Graduate Student Member, IEEE*, Ning Pan, *Graduate Student Member, IEEE*, Dominique Schreurs, *Fellow, IEEE*, and Sofie Pollin, *Senior Member, IEEE*

***Abstract*— Simultaneous wireless information and power transfer (SWIPT) is gaining interest as it enables receivers with smaller batteries or none at all. However, the information and power transfer subsystems influence each other's performance, resulting in a tradeoff. SWIPT receivers should be low power and compact, ideally resulting in an energy-efficient design where hardware is maximally shared between information and power reception blocks. We propose a novel frequency-shift keying (FSK) modulation scheme that uses waveforms that are known to improve wireless power transfer efficiency and can be decoded by relying on the nonlinearity of the energy harvesting hardware. This hardware sharing saves area and avoids using a local oscillator (LO). We analyze two novel multitone FSK schemes while presenting measurement results proving the feasibility of the proposed schemes. Information transfer is based on the relationship between input frequency spacings and rectifier output intermodulation product frequencies. We show that contrary to the existing amplitude variation-based modulation schemes for SWIPT, the symbol rate for uniform multitone FSK in the noiseless case is not limited by the rectifier low-pass filter. For our proposed nonuniform multitone FSK scheme, the symbol rate is limited but spectral efficiency is much higher. We show by measurements that information transfer of at least 18 Mb/s using the rectifier as a receiver is feasible, which is a large increase compared to other solutions. A proposed optimization increases feasible symbol rate for the nonuniform FSK scheme by at least a factor of four.**

***Index Terms*— Energy harvesting, frequency shift keying (FSK), receiver architecture, simultaneous wireless information and power transfer (SWIPT), wireless power transfer (WPT).**

I. Introduction

SIMULTANEOUS wireless information and power transfer (SWIPT) is the combination of wireless information transfer (WIT) and wireless power transfer (WPT). SWIPT is a promising solution to lower the dependency on batteries of sensors, for example, in an Internet-of-Things (IoT) network. WIT has been studied extensively. Far-field WPT research, however, has recently gained some attention with the research community focusing on different aspects of a WPT system, trying to improve radio frequency (RF)-to-dc power conversion efficiency (PCE) as much as possible. The waveform is also shown to strongly impact PCE. The works in [1]–[7] showed that high peak-to-average power ratio (PAPR) waveforms improve PCE at low input power levels for far-field, radiative WPT. Multitone signals are popular WPT waveforms since their PAPR can easily be controlled by varying the amount of tones. Recently, multisine signals were also adopted for near-field WPT systems [8], which typically uses single-tone signals, modulated with amplitude-shift keying (ASK), phase-shift keying (PSK), frequency-shift keying (FSK), or pulsewidth modulation (PWM) [9], [10]. When adopting WPT efficiency increasing multitone signals, however, these single-tone modulation techniques need adaptation. Hence, this work proposes a multitone version of classical FSK, where the information is in the distance between tones, enabling power optimized multisine signals for WPT that can be received without LO. The technique is demonstrated using far-field WPT hardware but is also applicable in near-field applications.

Despite the research on both topics, combining both the WIT and WPT subsystems remains a challenging topic, especially when the waveform is shared to simultaneously carry both power and information. The receiver can have separated paths for power and information or integrated paths [11]. Since RF power harvesting is limited due to regulatory constraints and PCE limits, the sensor should be low power. Hence, modulation techniques that enable SWIPT receivers with limited hardware and an alternative for the power-consuming LO are very desirable since the considerable decrease in power consumption of the SWIPT receivers [11]. In addition, the SWIPT waveform should adopt the WPT waveform optimizations, so it should have a high PAPR character. Also, it has been shown that there exists a strong mutual impact between both subsystems, which should be taken into account when designing SWIPT modulation techniques [12]. For example, a measurement-based analysis in [12] showed that for a SWIPT system, WIT performance degrades when high PAPR waveforms are modulated with, for example, PSK or quadrature ASK. This is because of transmitter nonlinearity, which causes distortion, especially when transmitting high PAPR waveforms at high power levels. Hence, concerning modulation and waveforms, there is a lot of room for improvement, when comparing to a classical ASK-modulated carrier for SWIPT.

Recent work has advanced the practical study of unconventional, optimized SWIPT modulation techniques that can be received without LO. First, the work in [13] introduced a modulation technique that leverages the PCE improvement of multitone signals and its relationship between the number

Manuscript received August 31, 2018; revised December 29, 2018 and February 23, 2019; accepted March 3, 2019. Date of publication April 22, 2019; date of current version May 6, 2019. This work was supported in part by the Fonds voor Wetenschappelijk Onderzoek (FWO) and in part by the Hercules Foundation. This paper is an expanded version from the IEEE Wireless Power Transfer Conference, Montreal, QC, Canada, June 3–7, 2018. *(Corresponding author: Steven Claessens.)*

The authors are with the TELEMIC Division, ESAT, Katholieke Universiteit Leuven, 3000 Leuven, Belgium (e-mail: steven.claessens@kuleuven.be; ning.pan@kuleuven.be; dominique.schreurs@kuleuven.be; sofie.pollin@kuleuven.be).

Color versions of one or more of the figures in this paper are available online at http://ieeexplore.ieee.org.

Digital Object Identifier 10.1109/TMTT.2019.2908645

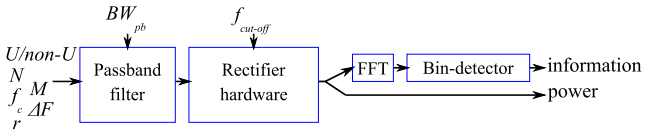

Fig. 1. Receiver system diagram for receiving the proposed multitone FSK modulation scheme using FFT.

of tones and PAPR. The information is encoded in the number of tones, while PAPR is measured at the rectifier output. Next, Claessens *et al.* [14], [15] optimized SWIPT waveforms by proposing a biased ASK modulation scheme where each symbol is ensured to carry some minimum power, trading of WIT for WPT. Finally, the works in [16] and [17] proposed encoding the information in the amplitude or phase ratio between two tones of a multitone signal. However, these modulation techniques either impact the rectifier output amplitude in some way or limit the number of input tones, risking high-amplitude variations.

As a solution, we investigated, in [18], the possibility of encoding information in the two-tone signal's frequency spacing in order to limit this impact. In addition, the output power is shown to increase and be more stable for a high ratio ($F_{\text{ratio}} = \Delta f/f_{\text{cut}}$) between the symbol rate and the rectifier's cutoff frequency [12], [19], so a modulation technique that is still decodable by the rectifier at high F_{ratio} is desirable. FSK is a classical technique for WIT. However, it limits the signal to a single tone, which does not optimize PCE. In [18], we extended the FSK technique to two tones and encode the information not in the tones' frequency but in the frequency spacing between the tones. The reason is that the intermodulation products' frequencies at the rectifier output are related to the frequency spacings of the input signal [20]. The information can be decoded without a LO by simply detecting the second intermodulation product's frequency at the rectifier output using the system depicted in Fig. 1. This two-tone FSK technique allows for the transmission of information while optimizing PCE by using a multitone signal. Our two-tone FSK technique was shown to increase this decodable F_{ratio} limit, compared to the biased ASK technique. Yet, the proposed novel modulation technique in [18] was based on, and limited to, only two tones, posing a limit on PCE since PAPR is limited to four.

In order to alleviate this limitation, this paper is an extension of our two-tone FSK technique in [18], providing two novel practical solutions to increase the number of tones while still encoding information in the signal's frequency spacing, using multitone FSK for SWIPT.

The first proposed multitone FSK technique in this paper varies the frequency spacing between all N tones at the same time. This is why we call it uniform multitone FSK. It is a straightforward increase in the number of tones, starting from our two-tone FSK modulation technique proposed in [18], allowing for higher PAPR waveforms.

The second proposed technique is called nonuniform FSK since the frequency spacings between different tones are not the same. This lowers the amount of tones in a certain bandwidth, lowering WPT, but increases spectral efficiency as we will show later in this paper. Hence, both PAPRs are increased and spectral efficiency is increased compared to the two-tone FSK modulation technique proposed in [18].

Both techniques encode information in the frequency spacing between tones, resulting in sets of multisine symbols with constant PAPR and lowering the impact of WIT on WPT efficiency.

This novel and the aforementioned LO-less SWIPT modulation techniques rely on the diode for downconversion, rendering the channel highly nonlinear. For these types of channel, the classical Shannon capacity bound is inaccurate [21]. Nevertheless, the relationship between system parameters and optimal throughput is analyzed in detail in this paper. Because of the channel nonlinearity and the fact that no power splitting or time switching is applied, existing optimizations for SWIPT systems, such as resource allocation [22], power splitting and time switching optimizations [23], and optimizations of modulation techniques that require an LO at the receiver [24], need revision, and new optimizations are likely to arise in the near future to further improve performance of such integrated LO-less SWIPT systems. For example, multiple modulation techniques could be combined in multimode SWIPT, depending on the environmental and operating conditions like the power level [25].

The rest of this paper is organized as follows. Section II describes the receiver including the model for simulations and hardware setup for measurements. In Section III, we present both the uniform and nonuniform versions of multitone FSK as novel modulation techniques for SWIPT. Simulations and experimental analysis of both schemes are presented in Sections IV and V, respectively. Next, we propose an optimization to improve performance in Section VI, followed by the conclusion in Section VII.

II. Receiver Model

The system model is shown in Fig. 1. This topology consists of an input matching network, and a diode followed by an *RC*-low-pass filter (LP-filter), a Fourier transformation [fast Fourier transform (FFT)], and a bin-detector block. A passband filter is placed in front of the rectifier to filter out unnecessary noise and interference. In practical realizations, a passive filter bank could be implemented to realize the FFT operation and further decrease power consumption. The FFT and bin detector are used to demodulate the signals after the integrated rectifier. The bin detector compares for each symbol the energy levels of the baseband (BB) bins to find the strongest intermodulation products. Optimizing the hardware and system parameters for WPT limits WIT since ripple and information content will decrease and the rectifier will attenuate the BB bins nonuniformly.

The considered transmitted signal can be described by

$$S_{\text{in}}(t) = \sum_{i=1}^{N} \cos(2\pi t \times f_{\text{tone}}(i)) \tag{1}$$

where N is the number of tones and $f_{\text{tone}}(i)$ will be defined in (2) and (3) for the uniform and nonuniform schemes, respectively. The signal $S(t)$ is a sequence of symbols.

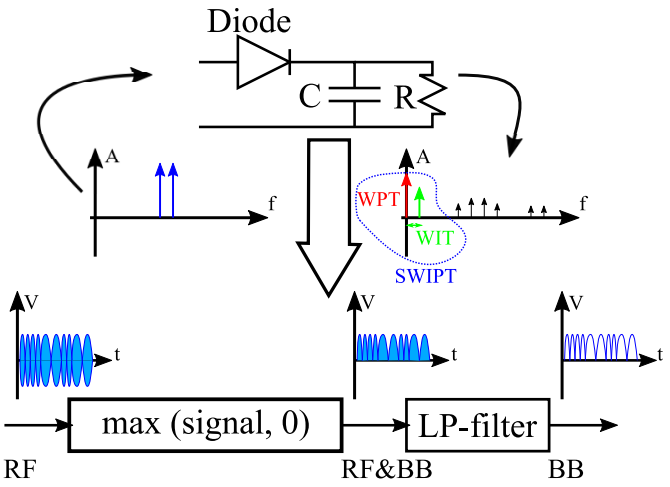

Fig. 2. Circuit model (top) and system model (bottom) for the rectifier hardware, demonstrating the coexistence of a power and IM_2 tone, indicating RF and BB signals.

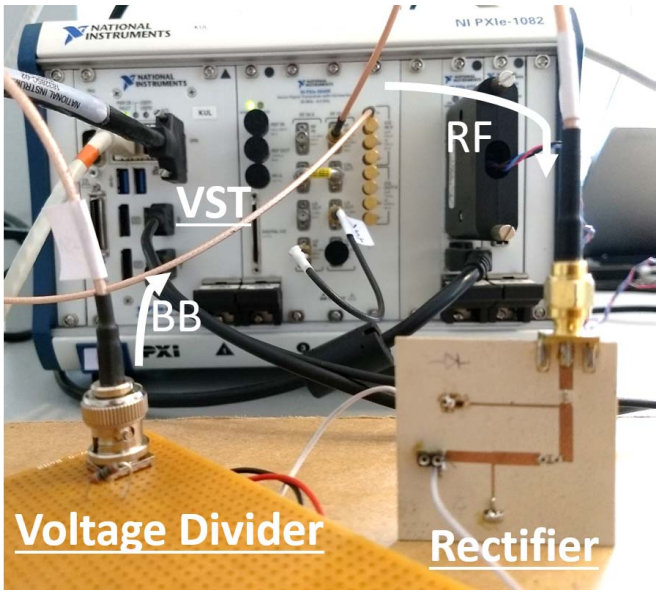

Fig. 3. Measurement setup with VST, rectifier, and voltage divider.

While the duration of each symbol is constant, they each have a unique set of $f_{\text{tone}}(i)$. The diode is simulated by a basic switch model for simulations, and the LP-filter is modeled by transfer function H in (18). Hence, the simulated output signal could be described by $S_{\text{out}}(t) = H(\max(0, S_{\text{in}}(t)))$.

A. Simulation Model

In this work's simulations, a simple model, which is commonly used in communication theory textbooks, is used to represent the rectifier envelope detector hardware. The diode is considered to behave as a zero-threshold switch, which stops negative signals but passes positive signals. The diode is followed by an *RC*-LP-filter, as shown in Fig. 2. This model was also used in [14] and [15] where the simulation results based on this model was shown to approximate WIT measurement results when considering a (biased) ASK modulation for SWIPT applications. In this model, the LP-filter and diode are assumed to be independent, meaning that loading effects are ignored.

The rectifier's LP-filter consists of a parallel resistor and a capacitor. The rectifier's cutoff frequency is f_{cut}.

B. Experimental Setup

The measurement results presented in this section verify the relationship between the input symbol and output second-order intermodulation (IM_2) tones and its ability to use them as described in our proposed multitone FSK scheme. The measurements are performed using a vector signal transceiver (VST) (NI PXIe-5645R) for transmitting the 2.45-GHz RF signals. Its RF output is connected to a rectifier that consists of one diode and an *RC*-LP-filter. Rectifier specifications are described in [26]. The rectifier's output is connected to the VST's BB input port using a small voltage divider circuit to avoid loading effects. This setup is shown in Fig. 3. Symbol error rate (SER) and output voltage are measured while varying the modulation parameters in order to study the tradeoff between both.

III. Signal Model

We propose two multitone FSK SWIPT modulation schemes: uniform multitone FSK and nonuniform multitone FSK. Both schemes are based on the relationship between multitone's frequency spacings and the rectifier output's intermodulation product's frequencies. Only the frequency spacings are varied, assigning constant and uniform amplitude and phase to all tones in both schemes. The two schemes are discussed in Sections III-A and III-B.

A. Uniform Multitone FSK

The idea of uniform multitone FSK is that when transmitting a multitone signal with N tones and uniform frequency spacing Δf between tones, the rectifier output will contain a strong frequency component (IM_2) at frequency Δf, as shown in Fig. 2. Hence, when varying the frequency spacing of the input signal, IM_2 will also shift frequency, which is detectable by using an FFT. This described scheme is called uniform multitone FSK since the frequency spacing between all neighboring tones is the same (multiple of) Δf.

We have demonstrated the feasibility of the uniform two-tone FSK scheme in [18]. This scheme can be extended to more tones, which is desirable for WPT since input PAPR will increase. For WIT, however, there will not only be one IM_2 tone present at the rectifier output. A lot of different intermodulation products at frequencies, which are multiples of the frequency spacing, will occur since not only neighboring tones intermodulate. This poses a challenge in detecting IM_2 with the detector shown in Fig. 1. The feasibility of such a uniform multitone scheme depends on the assumption that, for example, for the first symbol, IM_2 at $f = \Delta f$ is the strongest in amplitude, which is expected since its amount of intermodulating tone pairs in the input signal is the highest.

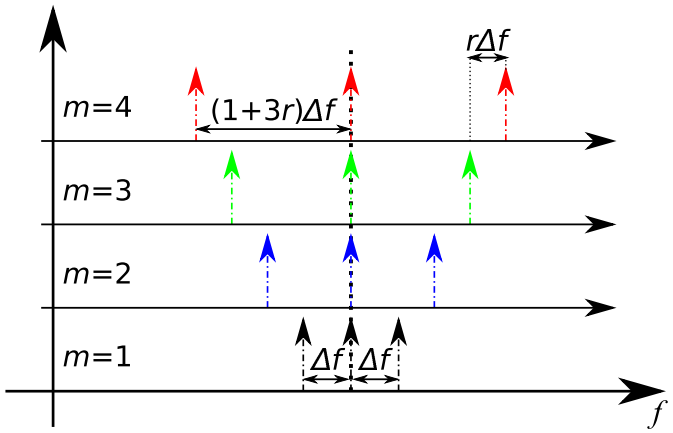

Fig. 4. Signal model illustrating the symbol construction for the proposed novel uniform FSK scheme, illustrated for three tones and M=4.

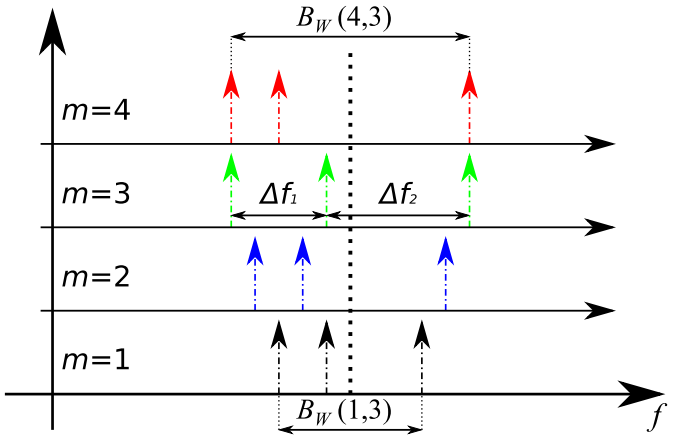

Fig. 5. Signal model illustrating the symbol construction for the proposed novel nonuniform FSK scheme, illustrated for three tones and M=4.

The uniform multitone FSK frequencies are mathematically determined by

$$f_{\text{tone}}(n, m, M, r, \Delta f) = f_c + \left(\frac{1+mr}{2}\right)\Delta f \times (2n-N-1), \quad \text{for } 1 \le n \le N \quad \text{for } 0 \le m \le M-1 \tag{2}$$

where r is the change in frequency spacing between different symbols, n is the tone index starting on the left in the spectrum, N is the total amount of tones, M is the modulation order, and m is the symbol index. This proposed uniform modulation scheme is shown in Fig. 4 for a three-tone signal and $M = 4$. The figure clearly shows how different symbols are constructed by only changing the frequency spacings in the same way.

In this uniform scheme, we can increase the amount of tones while still keeping the frequency spacing the same between all tones. This restriction can be lifted to increase spectral efficiency for WIT while still using multiple tones for WPT. We call this nonuniform multitone FSK, which is introduced next.

B. Nonuniform Multitone FSK

In the nonuniform multitone FSK scheme, frequency spacings between neighboring tones are not the same. WPT is expected to be lower since the bandwidth is not optimally, or maximally, filled with tones, but WIT is expected to improve since the amount of bits per symbol increases, increasing spectral efficiency as shown later. For the uniform multitone FSK scheme, for example, for the first symbol, $N-1$ intermodulating tone pairs contribute to IM_2 at $f = \Delta f$ while $N-2$ intermodulating tone pairs contribute to the intermodulation product at twice that frequency and so forth. In this nonuniform multitone FSK scheme, this is not the case since different frequency spacings are used within one symbol. This proposed nonuniform modulation scheme is illustrated in Fig. 5 for a three-tone signal and $M = 4$.

The nonuniform multitone FSK scheme is constructed by choosing tones with different frequency spacings. The amount of frequency spacings considered for N tones is $N(N-1)/2$. These are chosen to assure that the resulting intermodulation products are all located at different frequencies in order to easily detect the original signal based on the rectifier output. Instead of a mathematical solution, we find the desired tone distribution in terms of N by exhaustive search. The frequency spacings for nonuniform three-, four-, and five-tone FSK are presented, from left to right, in Tables I–III, respectively. The tables show the symbol frequency spacings, normalized to Δf, for a modulation order up to $M = 8$. Moreover, higher orders are possible. These sets of frequency spacings result in sets of unique, noncoinciding IM_2 tones at the rectifier output in BB.

TABLE I
FREQUENCY SPACINGS ($\Delta f_i(m, N = 3)$) FOR NONUNIFORM THREE-TONE FSK, NORMALIZED TO Δf

m	$\Delta f_1'(m,3)$	$\Delta f_2'(m,3)$
1	1	2
2	1	3
3	2	3
4	1	4
5	2	4
6	1	5
7	2	5
8	3	4
...		

TABLE II
FREQUENCY SPACINGS ($\Delta f_i(m, N = 4)$) FOR NONUNIFORM FOUR-TONE FSK, NORMALIZED TO Δf

m	$\Delta f_1'(m,4)$	$\Delta f_2'(m,4)$	$\Delta f_3'(m,4)$
1	1	3	2
2	1	2	4
3	1	4	2
4	2	1	4
5	1	2	5
6	1	4	3
7	1	5	2
8	2	1	5
...			

TABLE III
FREQUENCY SPACINGS ($\Delta f_i(m, N = 5)$) FOR NONUNIFORM FIVE-TONE FSK, NORMALIZED TO Δf

m	$\Delta f_1'(m,5)$	$\Delta f_2'(m,5)$	$\Delta f_3'(m,5)$	$\Delta f_4'(m,5)$
1	1	3	5	2
2	2	5	1	3
3	1	3	6	2
4	1	6	2	3
5	2	6	1	3
6	1	3	7	2
7	1	4	6	2
8	1	5	3	4
...				

The nth tone's frequency for nonuniform multitone FSK can be found from these frequency spacings, using

$$f_{\text{tone}}(n, m, N, M, \Delta f) = f_c - \frac{B_W(m, N)}{2} + \sum_{i=1}^{n-1} \Delta f_i(m, N), \quad \text{for } 1 \le n \le N, \quad \text{for } 1 \le m \le M \tag{3}$$

with tone index n starting on the left of the spectrum, N is the total number of tones, $\Delta f_i(m, N)$ is the nonnormalized frequency spacing, m is the symbol index, and $B_W(m, N)$ is the symbol bandwidth determined by

$$B_W(m, N) = \sum_{i=1}^{N-1} \Delta f_i(m, N), \quad \text{for } 1 \le i \le N-1. \tag{4}$$

These tone distributions result in $N(N-1)/2$ BB tones. Of these, $N-1$ are located at frequencies equal to the frequency spacings $\Delta f_i(m, N)$. There are also additional intermodulating tones created at frequencies equal to

$$f_{\text{IM}}(m, N, i, k) = \sum_{j=i+1}^{k} \Delta f_j(m, N) + \Delta f_i(m, N), \quad \text{for } 1 \le i \le N-1, \quad \text{for } i+1 \le k \le N-1. \tag{5}$$

The set of intermodulation products at frequencies, which equal the frequency spacings in Tables I–III, and the additional intermodulation products determined by (5), are unique for each symbol. Hence, WIT is enabled by recognizing symbols at the rectifier output by detecting the set of intermodulation products.

IV. ANALYSIS OF UNIFORM MULTITONE FSK

In this section, a mathematical analysis of uniform multitone FSK is presented, leading to the expression for spectral efficiency. This is followed by experimental results, demonstrating the feasibility and limitations of the scheme.

A. Theoretical Analysis

After the signal is downconverted by the rectifier hardware, an FFT operation is performed. The only requirement to receive a signal modulated by the proposed uniform multitone FSK scheme is to detect IM_2's frequency, which is known to be one of the M values. Although BB versions of the classical noncoherent FSK receivers can still be used, they are less flexible, and the implementation in an integrated SWIPT receiver is less straightforward compared to an FFT-based approach. Hence, we elaborate on an FFT-based receiver. We investigate the inherent relationship between the throughput and the bandwidth, extending this relationship for two tones, which we already established in [18].

The bandwidth of the uniform FSK-modulated multisine is defined as

$$B_W = (1 + (M-1)r)\Delta f(N-1) + 0.5r\Delta f. \tag{6}$$

The center frequencies of the FFT-bins f_{bin} are expressed by

$$f_{\text{bin}}(i) = \frac{F_s}{L} \times i, \text{ with } -\frac{L}{2} \le i \le \frac{L}{2} \tag{7}$$

where i is an integer bin index, L is the number of samples in one symbol over which the FFT is taken, and F_s is the sampling rate. The symbol size L is expressed in terms of the amount of BB periods n in one symbol

$$L = \frac{F_s}{\Delta f} \times n. \tag{8}$$

The width of one FFT frequency bin (B_w) can be found by combining (7) and (8) and equals

$$B_w = \frac{F_s}{\frac{nF_s}{\Delta f}} = \frac{\Delta f}{n}. \tag{9}$$

The FFT's frequency resolution has to be precise enough to ensure that the frequency shifts at the rectifier's output, as described in Section III, can be detected. This results in a constraint on the maximal bin width, expressed by

$$B_w = \gcd(1, r)\Delta f \tag{10}$$

where gcd(,) is the greatest common divider operation. Since r can be rational, we assume that $\gcd(1, r = 0.5) = 0.5$ and $\gcd(1, r = 1.5) = 0.5$. The FFT bin width determined by the amount of BB periods per symbol is expressed by (9). The maximal bin width determined by the detectable frequency shifts is expressed by (10). The relationship between necessary amount of BB periods per symbol and detectable frequency shift is found by combining these two equations, resulting in

$$n_{\min} = \frac{1}{\gcd(1, r)}. \tag{11}$$

This illustrates that the FFT has to be taken over more symbols to be precise enough to detect small frequency shifts, which will result in a relationship between the bandwidth and throughput as is shown next. The relation in (11) also ensures that different locations for IM_2 align with the bins' center frequencies in (7). The ideal information throughput is expressed by

$$T_P = \frac{\log_2(M)}{T_{\text{symb}}} \tag{12}$$

where symbol duration $T_{\text{symb}} = n/\Delta f$. The throughput for the uniform scheme, in (12), is independent of N since the frequency spacings are uniform and dependent and do not encode

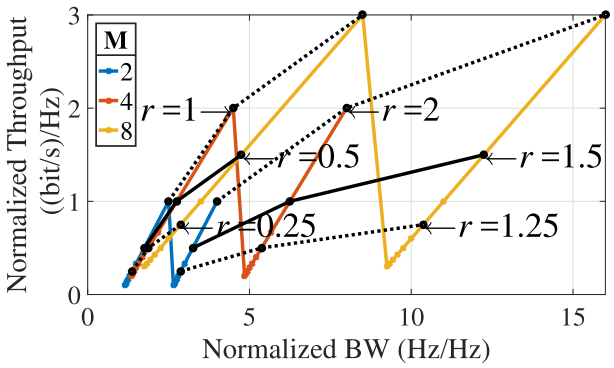

Fig. 6. Theoretical maximal throughput compared to bandwidth (B_W), normalized to ΔF for reasonable r, for an FFT-based detector and the proposed uniform FSK modulation scheme, with two tones.

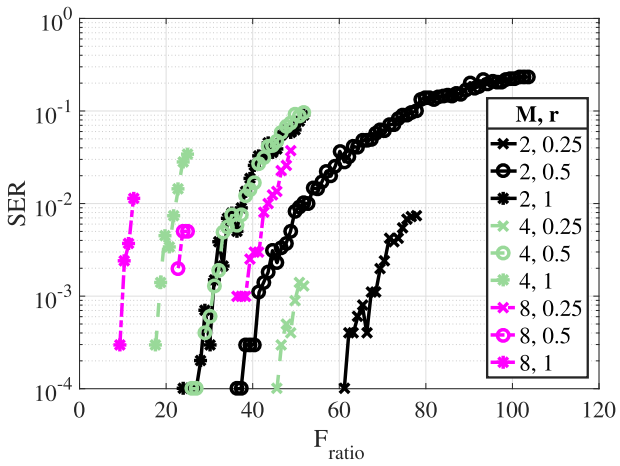

Fig. 7. Measurement results for SER, in terms of F_{ratio} with transmit power of 0 dBm, before improved signal processing, which theoretically removes the limiting F_{ratio}.

individual information. This is different for the nonuniform scheme as will be shown in (15). The maximal throughput $T_{\text{P,max}}$ is found by substituting (11) in (12), resulting in

$$T_{\text{P,max}} = \gcd(1, r) \log_2(M) \Delta f. \tag{13}$$

The relationship between the maximal throughput and bandwidth is found by combining (6) and (13)

$$S_{\text{E,max}} = \frac{\gcd(1, r) \log_2(M)}{(1 + (M-1)r)(N-1) + 0.5r}. \tag{14}$$

By controlling the range of frequency spacings with M and r, it is possible to control the throughput and PCE. Fig. 6 confirms that $r = 1$ results in the largest possible throughput for each modulation order and used bandwidth. This figure shows the relationship between the maximal throughput and bandwidth, both normalized to ΔF. A low two-tone FSK modulation order is shown to be beneficial when high spectral efficiency and low bandwidth are desired. Taking r=1 gives the maximum throughput and spectral efficiency, however, r can be lowered to further tradeoff spectral efficiency and power. This is because for small r, the frequency spacing does not change a lot for different symbols, which leads to symbols with more power efficiency. This is because it is known that PCE increases with F_{ratio}, as shown in Fig. 7. This is because of more power efficient symbols with tones at the spectrum edges. Fig. 6 also shows that r should be a rational number between zero and one, which is the considered region in the rest of this paper. The data clearly indicate that the throughput for some $r > 1$ can also be achieved with lower bandwidth if $r < 1$. r should be rational because of the gcd operator in (10). The results for some rational $r < 1$ are indicated by dots in Fig. 6. For nonrational $r < 1$, $\gcd(1, r)$ would be very low, resulting in very low throughput, which is not shown in the figure because it is not an optimal parameter choice.

B. Experimental Analysis

In this section, we introduce the measurement results for uniform FSK modulation for SWIPT. Both power level and symbol rate are varied for different number of tones and modulation order.

Fig. 7 shows the suboptimal SER measurement results that we presented in [18], for varying modulation order M, frequency shift r, and F_{ratio}. Measurements are taken over 10^3 and 10^4 symbols, depending on the required bandwidth and available hardware sample rate. The results show that SER increases for increasing F_{ratio}. SER increases more with higher F_{ratio}, for higher M, and higher r. When using M =2 and r =0.25, SER is still below 10^{-4} for $F_{\text{ratio}} = 60$. Two-tone FSK with r =1 is shown here to enable a throughput of 5.79, 6.95, and 5.78 Mb/s at 10^{-3} SER for M =2, 4, and 8, respectively. This shows a five times increased throughput, compared to the biased ASK approach that was proposed in [14] and [15] while enabling the use of two-tone signals for efficient WPT. Also, choosing r smaller than 1 lowers SER since it avoids that higher order intermodulation products fall inside the IM_2 bins which would confuse the detector in noisy situations and for high F_{ratio}. A low r also results in less difference in attenuation of the bins by the hardware since they are closer together. It is important to note that after improving the signal processing in the receiver, the limits on F_{ratio} depicted in Fig. 7 drastically increase. Because of transmitter hardware limitations, measurements were only possible up to $\Delta f = 60 * 10^5$ Hz. This corresponds to throughputs of 6, 12, and 18 Mb/s at 0 SER for M =2, 4, and 8, respectively. Hence, in a noiseless case, WIT bitrate using uniform frequency spacings is not limited by F_{ratio}. In addition, measurements for varying number of tones from 2 to 32 also show that this unlimited character is not affected by the number of tones, which is very beneficial for WPT. This conclusion is also confirmed by simulations using the model shown in Fig. 2. Both observations are major benefits over the biased ASK modulation scheme that we proposed earlier in [14] and [15] where F_{ratio} was roughly limited to 20. However, increasing F_{ratio} leads to small output intermodulation products, which are very sensitive to noise. For a uniform two-tone FSK signal with certain fixed noise level and $F_{\text{ratio}} = 3$, measurements show that SER = 0.049, 0.135, and 0.400 for $M = 2, 4$, and 8, respectively. This demonstrates that also these schemes are more sensitive to noise with increasing modulation order.

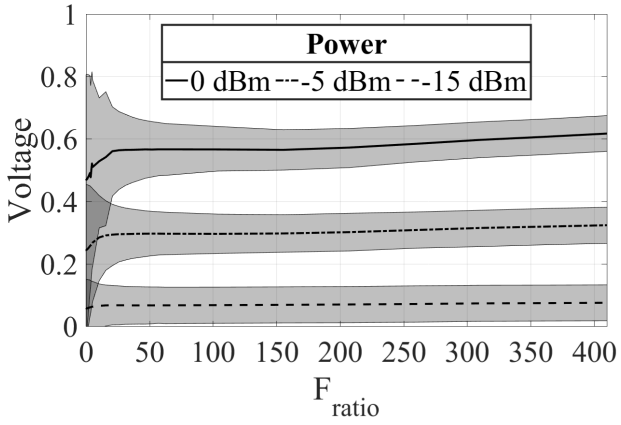

Fig. 8. Measurement results for rectifier output voltage swing (gray areas) and mean output voltage (solid lines) for a two-tone in-phase input signal, in terms of F_{ratio}, with transmit power of 0, −5, and −15 dBm.

The measured rectifier output voltage behavior for a two-tone in-phase input signal with varying frequency spacing is shown in Fig. 8. These measurement results show that WPT benefits from a high symbol rate and frequency spacing, increasing the mean output voltage. Hence, taking M =2 is optimal for WPT, considering a certain available bandwidth. WPT can further be optimized by lowering the frequency shift with r to maximize Δf. However, this means that throughput will drop, as shown in Fig. 6. Increasing F_{ratio} also decreases the voltage swing, which is beneficial for a reliable output power, as shown in Fig. 8.

V. Analysis of Nonuniform Multitone FSK

In this section, a mathematical analysis of nonuniform multitone FSK is presented, leading to the expression for spectral efficiency. This is followed by experimental results, demonstrating the feasibility and limitations of the scheme.

A. Theoretical Analysis

The information throughput for nonuniform multitone FSK is expressed by

$$T_P = \frac{\log_2(M)(N-1)}{T_{\text{symb}}} \tag{15}$$

where symbol duration $T_{\text{symb}} = n/\Delta f$, M is the amount of symbols, and N is the number of tones per symbol. Here, the throughout does depend on the number of tones since N relates to the number of independent frequency spacings, which encode independent information. The maximal throughput $T_{\text{P,max}}$ is found by substituting (11) (with $r = 1$) in (15), resulting in

$$T_{\text{P,max}} = \log_2(M)(N-1)\Delta f. \tag{16}$$

The relationship between the maximal throughput and bandwidth depends on the number of symbols M and the number of tones per symbol N. Fig. 9 shows the bandwidth–throughput relationship, normalized to Δf, depending on the number of tones and modulation order, for nonuniform multitone FSK. WIT is optimized when choosing the parameter values that maximize spectral efficiency, the ratio of throughput over bandwidth. These points are indicated with black circles in Fig. 9. The optimal modulation orders M are [2], [2, 4], [4, 8, 16, 32, 64], [32, 64, 128, 256, 512, 1024], and [512, 1024, 2048] for 2, 3, 4, 5, and 6 tones, respectively.

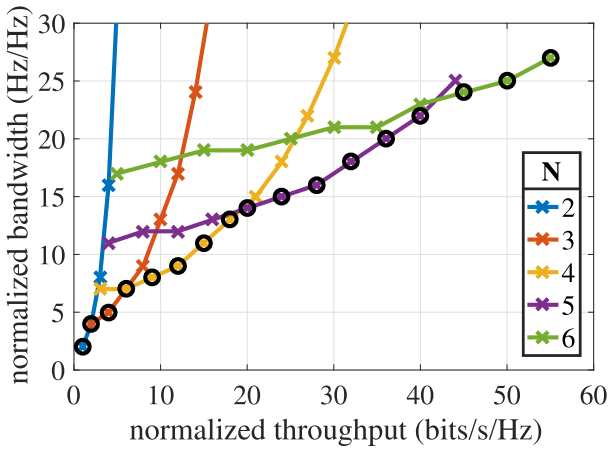

Fig. 9. Bandwidth–throughput relationship for nonuniform multitone FSK, both normalized to Δf, depending on number of tones and modulation order (from 2 to 2048, from left to right), with circles indicating the optimal selection of N and M concerning spectral efficiency.

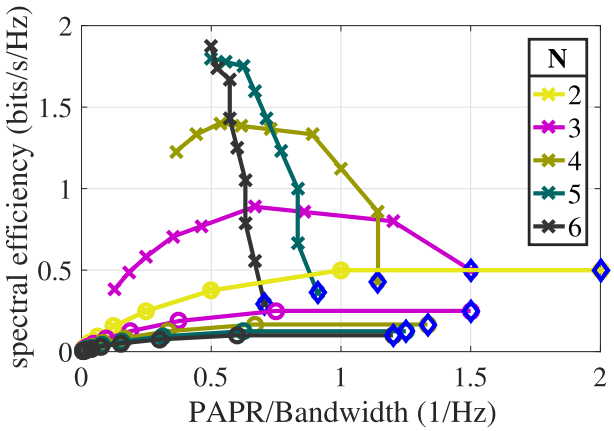

Fig. 10. Relationship between spectral efficiency and PAPR for uniform (circle) and nonuniform (crossed) multitone FSK, for various number of tones and modulation orders with the $M = 2$ case indicated by diamonds.

Numerically optimizing spectral efficiency (S_E) results in the following relationship between the bandwidth from (4), frequency spacing, and modulation order for the nonuniform scheme:

$$\begin{aligned} S_{\text{E,max}} &= \frac{\log_2(M)(N-1)\Delta f}{B_W} \\ &= 0.657 * \ln(\log_2(M)) + 0.435. \end{aligned} \tag{17}$$

This theoretical analysis of nonuniform multitone FSK and the analysis for uniform multitone FSK in Section IV are summarized Fig. 10. This figure shows the tradeoff between spectral efficiency, desired for WIT, and PAPR, desired for WPT. It is clear that nonuniform FSK results in better spectral efficiency, whereas the uniform scheme fills the bandwidth more, resulting in higher PAPR. However, as will be shown in the next section, WIT using the uniform scheme can use a much higher F_{ratio}, improving WPT as well as throughput, which is certainly useful in some applications.

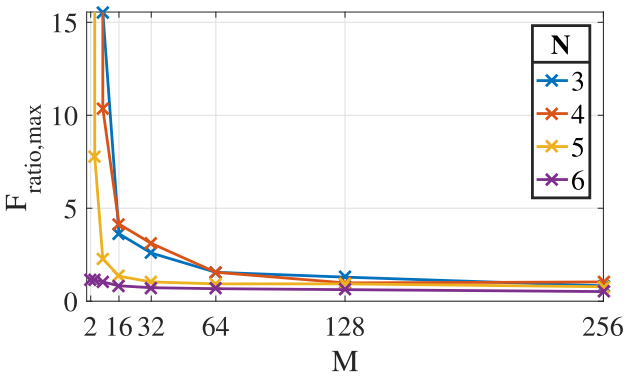

Fig. 11. Measurement results for nonuniform multitone FSK, demonstrating the upperbound on F_{ratio} for different number of tones N and modulation order M.

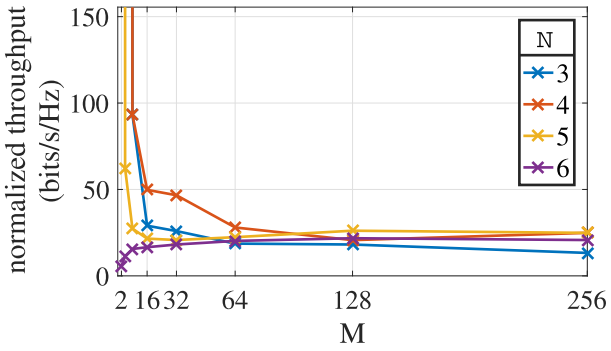

Fig. 12. Measurement results for nonuniform multitone FSK, demonstrating the upperbound on throughput for different number of tones N and modulation order M, normalized to the LP-filter's cutoff frequency.

B. Experimental Analysis

Fig. 11 shows the measured F_{ratio} upperbound results for nonuniform FSK modulation for our specific rectifier while varying the number of tones and modulation order. The results show that F_{ratio} needs to drop for increasing the number of tones and increasing the modulation order in order to still decode information. The main limiting factor is the nonuniform attenuation of the rectifier's LP-filter, leading to erroneous detection of the output set of intermodulation products. Hence, we can choose between the low symbol rate with high modulation order and high symbol rate with low modulation order. Both impact throughput. This limit for the nonuniform scheme is similar to the limit found for biased ASK in [14] and [15]. Contrary to the uniform scheme, F_{ratio} is limited for the nonuniform scheme and for (biased) ASK ([14], [15]), limiting throughput for a certain integrated rectifier receiver. However, (biased) ASK can be received more easily, without FFT, and the nonuniform scheme increases spectral efficiency, providing different tradeoffs depending on what the application needs. The realizable throughput, calculated from Fig. 11 using (16), is shown in Fig. 12, showing that for our rectifier, the highest throughput can be reached by choosing a low modulation order and less than six tones.

Fig. 12 shows the measured throughput upperbound results for nonuniform FSK modulation while varying the number of tones and modulation order, relative to the LP-filter's cutoff frequency, using (16). It is well known that the diode's nonlinear behavior is power dependent. Since our modulation schemes are based on that nonlinearity, it is worth investigating whether their performance is power dependent as well. The measurement results shown in Fig. 13 demonstrate the impact of power on the nonuniform scheme's F_{ratio} upperbound. The upperbound decreases for lower power level. This means that the proposed modulation technique is more useful at high power levels. A limiting factor (on F_{ratio}) is the unfair attenuation of the rectifier's LP-filter, causing errors in the bin-detection phase. As a solution, we propose an optimization in the next section.

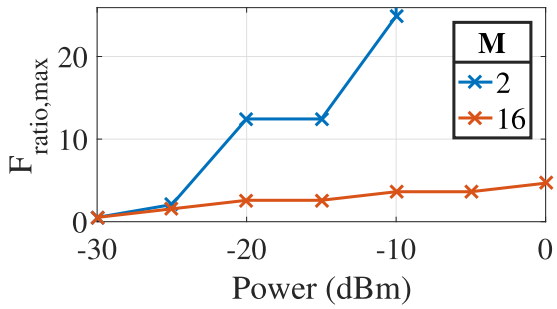

Fig. 13. Measurement results for the impact of input power on F_{ratio} upperbound, for a four-tone nonuniform FSK-modulated signal with varying modulation orders.

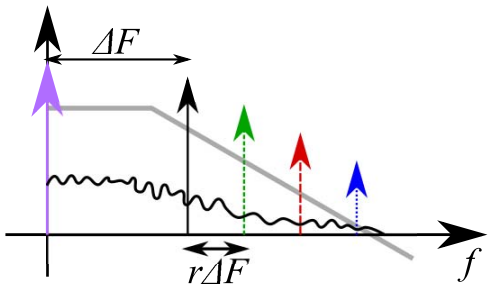

Fig. 14. Received signals in BB, after passing the rectifier, with different symbol outputs represented by different styles.

VI. Optimization

The LP-filter at the diode's output attenuates the BB frequency tones in a frequency-dependent way. This results in a different attenuation for different symbols since IM_2s are located elsewhere. This results in more errors for the symbols with high IM_2 frequency since they are attenuated more compared to the noise of intermodulation products in lower frequency bins. This is represented in Fig. 14 where each color represents a different symbol.

Measurement results presented earlier already showed that the uniform scheme is robust to this effect since only one BB tone is detected, and no other strong BB tones are present on the left of that tone. For the nonuniform scheme, however, a lot of different BB tones need to be detected, causing its sensitivity to this effect as presented earlier. Hence, a mathematical compensation is introduced to counter this effect. The ideal rectifier's LP-filter transfer function $H(i)$ is

$$H(i) = \frac{1}{1 + jF_{\text{ratio}}(1 + ri)}, \quad \text{for } 0 \leq i \leq M - 1 \qquad (18)$$

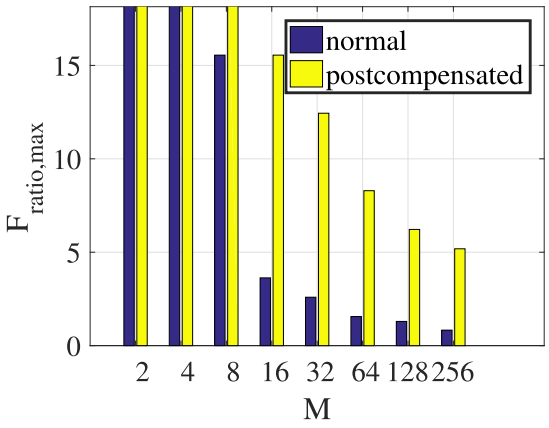

Fig. 15. Measurement results for F_{ratio} upperbound, with and without postcompensation, for a three-tone nonuniform FSK-modulated signal with varying modulation orders.

where i is the symbol index. A scaling factor for each bin is introduced in order to remove the unfair symbol attenuations before bin detection is performed. This individual scaling is determined by the bin's attenuation relative to the first bin. The bin scaling $K(i)$ is determined by

$$\frac{1}{K(i)}=\frac{|H(i)|}{|H(0)|}=\frac{\sqrt{1+(F_{\text{ratio}})^2}}{\sqrt{1+(F_{\text{ratio}})^2(1+ri)^2}},\quad \text{for } 0\le i\le M-1. \tag{19}$$

This mathematical compensation can be performed at the transmitter as precompensation of the signal or at the receiver as postcompensation. Both are discussed next. Our experiments in the next sections show that the compensation factors of (19) are not optimal in practice since they are based on an independent and ideal LP-filter. This means that one should look for the optimal bin weights, starting from the theoretical factors in (19) for a certain operating point to fully counter the LP-filter effect.

Applying these bin weights can be done both at the transmitter or receiver side, which is called precompensation and postcompensation, respectively. Both are discussed next.

A. Postcompensation

When considering postcompensation, the transmitted tones of all symbols have equal amplitude and phase. At the rectifier output, however, the LP-filter attenuates intermodulation products with higher frequency spacing more. This leads to detection errors. This unfair attenuation can be compensated for by rescaling the detected bins using (19). The measurement results shown in Fig. 15 demonstrate the huge benefit of applying postcompensation in the case of a three-tone nonuniform FSK-modulated signal.

B. Precompensation

The LP-filter can also be countered at the transmitter, using precompensation. In this case, the weights of (19) are applied when the symbols are generated. This scaling of each symbols results in a varying amplitude of the RF signal. This causes an undesired voltage ripple at the diode's output. However, it allows the receiver to be less complex. The RF-signal's PAPR, in the case of a uniform FSK modulation, is expressed by

$$\begin{aligned}&\text{PAPR}(N, M, F_{\text{ratio}}, r)\\ &\quad= 2N\times\frac{1+F_{\text{ratio}}^2(1+r(M-1))^2}{1+F_{\text{ratio}}^2}\\ &\quad=\frac{M\left(F_{\text{ratio}}^2((2M^2-3M+1)r^2+6(M-1)r+6)+6\right)}{6M\left(F_{\text{ratio}}^2+1\right)}\\ &\quad=\frac{12N(1+F_{\text{ratio}}^2(1+r(M-1))^2)}{\left(F_{\text{ratio}}^2((2M^2-3M+1)r^2+6(M-1)r+6)+6\right)}\end{aligned} \tag{20}$$

where N is the number of tones used and M is the modulation order. Since a standard multisine's PAPR is $2N$, (20) shows that PAPR increases.

VII. Conclusion

We propose two versions of a novel multitone FSK modulation technique for SWIPT, extending our proposed two-tone FSK modulation technique. This modulation scheme allows the information to be received by the rectifier hardware, without a power consuming LO. Information is encoded in the frequency spacings of multitone signals, allowing the usage of high PAPR signals for WPT while transferring information as well. The proposed uniform multitone FSK technique fills the bandwidth with tones, optimizing PAPR and hence WPT. The proposed nonuniform multitone FSK modulation technique still uses multitone signals but with varying frequency spacings between tones to increase the amount of information per symbol, increasing spectral efficiency and WIT performance. We show that these kinds of modulated signals allow to be downconverted using rectifier hardware, avoiding the need for a power-consuming LO. An optimization to counter the nonuniform LP-filter attenuation is proposed, increasing WIT even more in the nonuniform case. Our measurements show that both techniques perform well using a real power optimized rectifier. Both techniques allow to use high PAPR signals where each symbol carries both power and information, contrary to classical FSK and ASK. Our results show that the throughput of the uniform scheme is not limited by the rectifier hardware, contrary to (biased) ASK and the nonuniform scheme. However, (biased) ASK can be received more easily without FFT and the nonuniform scheme increases spectral efficiency.

In the future, it might be interesting to analyze and compare the impact of frequency-selective channels and corresponding precoders, as well as a typical mathematical rate-energy tradeoff comparison between these unconventionel SWIPT modulation techniques (multitone FSK, biased ASK, two-tone ratio modulation, and the PAPR modulation) and classical ASK and FSK.

References

[1] A. S. Boaventura and N. B. Carvalho, "Maximizing DC power in energy harvesting circuits using multisine excitation," in *IEEE MTT-S Int. Microw. Symp. Dig.*, Jun. 2011, pp. 1–4.

[2] A. Collado and A. Georgiadis, "Improving wireless power transmission efficiency using chaotic waveforms," in *IEEE MTT-S Int. Microw. Symp. Dig.*, Jun. 2012, pp. 1–3.
[3] C. L. Yang, C. L. Tsai, Y. L. Yang, and C. S. Lee, "Enhancement of wireless power transmission by using novel multitone approaches for wireless recharging," *IEEE Antennas Wireless Propag. Lett.*, vol. 10, pp. 1353–1357, Nov. 2011.
[4] A. Collado and A. Georgiadis, "Optimal waveforms for efficient wireless power transmission," *IEEE Microw. Wireless Compon. Lett.*, vol. 24, no. 5, pp. 354–356, May 2014.
[5] C. R. Valenta, M. M. Morys, and G. D. Durgin, "Theoretical energy-conversion efficiency for energy-harvesting circuits under power-optimized waveform excitation," *IEEE Trans. Microw. Theory Techn.*, vol. 63, no. 5, pp. 1758–1761, Apr. 2015.
[6] F. Bolos, J. Blanco, A. Collado, and A. Georgiadis, "RF energy harvesting from multi-tone and digitally modulated signals," *IEEE Trans. Microw. Theory Techn.*, vol. 64, no. 6, pp. 1918–1927, Jun. 2016.
[7] M. S. Trotter, J. D. Griffin, and G. D. Durgin, "Power-optimized waveforms for improving the range and reliability of RFID systems," in *Proc. IEEE Int. Conf. RFID*, Apr. 2009, pp. 80–87.
[8] Z. Liu, Z. Zhong, and Y.-X. Guo, "*In vivo* high-efficiency wireless power transfer with multisine excitation," *IEEE Trans. Microw. Theory Techn.*, vol. 65, no. 9, pp. 3530–3540, Sep. 2017.
[9] H.-J. Kim, H. Hirayama, S. Kim, K. J. Han, R. Zhang, and J.-W. Choi, "Review of near-field wireless power and communication for biomedical applications," *IEEE Access*, vol. 5, pp. 21264–21285, Sep. 2017.
[10] M. A. Hannan, S. M. Abbas, S. A. Samad, and A. Hussain, "Modulation techniques for biomedical implanted devices and their challenges," *Sensors*, vol. 12, no. 1, pp. 297–319, Dec. 2011.
[11] X. Zhou, R. Zhang, and C. K. Ho, "Wireless information and power transfer: Architecture design and rate-energy tradeoff," *IEEE Trans. Commun.*, vol. 61, no. 11, pp. 4754–4767, Nov. 2013.
[12] S. Claessens, M. Rajabi, N. Pan, S. Pollin, and D. Schreurs, "Measurement-based analysis of the throughput-power level trade-off with modulated multisine signals in a SWIPT system," in *Proc. 89th ARFTG Microw. Meas. Conf.*, Jun. 2017, pp. 1–4.
[13] D. I. Kim, J. H. Moon, and J. J. Park, "New SWIPT using PAPR: How it works," *IEEE Wireless Commun. Lett.*, vol. 5, no. 6, pp. 672–675, Dec. 2016.
[14] S. Claessens, D. Schreurs, and S. Pollin, "SWIPT with biased ASK modulation and dual-purpose hardware," in *Proc. IEEE Wireless Power Transf. Conf.*, May 2017, pp. 1–4.
[15] S. Claessens, N. Pan, M. Rajabi, D. Schreurs, and S. Pollin, "Enhanced biased ASK modulation performance for swipt with awgn channel and dual-purpose hardware," *IEEE Trans. Microw. Theory Techn.*, vol. 66, no. 7, pp. 3478–3486, Jul. 2018.
[16] M. Rajabi, S. Pollin, and D. Schreurs, "Hybrid rectifier-receiver node," in *IEEE MTT-S Int. Microw. Symp. Dig.*, Jun. 2017, pp. 1038–1041.
[17] M. Rajabi, N. Pan, S. Claessens, S. Pollin, and D. Schreurs, "Modulation techniques for simultaneous wireless information and power transfer with an integrated rectifier–receiver," *IEEE Trans. Microw. Theory Techn.*, vol. 66, no. 5, pp. 2373–2385, May 2018.
[18] S. Claessens, C.-M. Chen, D. Schreurs, and S. Pollin, "Massive MIMO for SWIPT: A measurement-based study of precoding," in *Proc. IEEE 19th Int. Workshop Signal Process. Adv. Wireless Commun.*, Jun. 2018, pp. 1–5.
[19] N. Pan, A. S. Boaventura, M. Rajabi, D. Schreurs, N. B. Carvalho, and S. Pollin, "Amplitude and frequency analysis of multi-sine wireless power transfer," in *Proc. Integr. Nonlinear Microw. Millim.-Wave Circuits Workshop*, Oct. 2015, pp. 1–3.
[20] S. A. Maas, "Two-tone intermodulation in diode mixers," *IEEE Trans. Microw. Theory Techn.*, vol. 35, no. 3, pp. 307–314, Mar. 1987.
[21] K. S. Turitsyn and S. K. Turitsyn, "Nonlinear communication channels with capacity above the linear Shannon limit," *Opt. Lett.*, vol. 37, no. 17, pp. 3600–3602, Sep. 2012.
[22] X. Xu, A. Özcelikkale, T. McKelvey, and M. Viberg, "Simultaneous information and power transfer under a non-linear RF energy harvesting model," in *Proc. IEEE Int. Conf. Commun. Workshops*, May 2017, pp. 179–184.
[23] W. Liu, X. Zhou, S. Durrani, and P. Popovski, "SWIPT with practical modulation and RF energy harvesting sensitivity," in *Proc. IEEE Int. Conf. Commun.*, May 2016, pp. 1–7.
[24] B. Clerckx, "Wireless information and power transfer: Nonlinearity, waveform design, and rate-energy tradeoff," *IEEE Trans. Signal Process.*, vol. 66, no. 4, pp. 847–862, Feb. 2018.
[25] J. JinPark, J. HoMoon, K.-Y. Lee, and D. InKim, "Adaptive mode switching algorithm for dual mode SWIPT with duty cycle operation," in *Proc. IEEE 19th Int. Workshop Signal Process. Adv. Wireless Commun.*, Jun. 2018, pp. 1–5.
[26] T. J. Lee, P. Patil, C. Y. Hu, M. Rajabi, S. Farsi, and D. M. M.-P. Schreurs, "Design of efficient rectifier for low-power wireless energy harvesting at 2.45 GHz," in *Proc. IEEE Radio Wireless Symp.*, Jan. 2015, pp. 47–49.

Steven Claessens (GS'16) received the B.Sc. and M.Sc. degrees in electrical engineering from Katholieke Universiteit (KU) Leuven, Leuven, Belgium, in 2014 and 2016, respectively. He is currently pursuing the Ph.D. degree with a focus on simultaneous wireless information and power transfer, including waveform design, backscattering, and massive multiple-in multiple-out (MIMO) processing at KU Leuven.

Ning Pan (GS'16) was born in Dongyang, China, in 1989. She received the B.Sc. degree in electronic and information engineering with a focus on underwater acoustics from the Harbin Engineering University, Harbin, China, in 2011, and the M.Sc. degree in electrical engineering from the Delft University of Technology, Delft, The Netherlands, in 2014. She is currently pursuing the Ph.D. degree in electrical engineering at Katholieke Universiteit Leuven, Leuven, Belgium.

Her current research interests include simultaneous wireless information and power transfer, nonlinear device modeling, resource allocation, and green networks.

Ms. Pan was a recipient of the Best Student Paper Award of WPTC 2017.

Dominique Schreurs (S'90–M'97–SM'02–F'12) received the M.Sc. degree in electronic engineering and the Ph.D. degree from Katholieke Universiteit (KU) Leuven, Leuven, Belgium.

She has been a Visiting Scientist with Agilent Technologies, Santa Rosa, CA, USA; ETH Zurich, Zurich, Switzerland; and the National Institute of Standards and Technology, Boulder, CO, USA. She is currently a Full Professor with KU Leuven, where he also the Chair of the Leuven LICT. Her current research interests include the microwave and millimeter-wave characterization and modeling of transistors, nonlinear circuits, and bioliquids, and system design for wireless communications and biomedical applications.

Dr. Schreurs was an IEEE MTT-S Distinguished Microwave Lecturer. She is currently the President of the IEEE Microwave Theory and Techniques Society. She was the General Chair of the 2007, 2012, and 2018 ARFTG Conferences and is currently the President of the ARFTG organization. She was the Editor-in-Chief of the IEEE TRANSACTIONS ON MICROWAVE THEORY AND TECHNIQUES.

Sofie Pollin (S'03–M'06–SM'14) received the Ph.D. degree (Hons.) from Katholieke Universiteit (KU) Leuven, Leuven, Belgium, in 2006.

From 2006 to 2008, she was with the University of California at Berkeley, Berkeley, CA, USA, where she was involved in the research on wireless communication, energy-efficient networks, crosslayer design, coexistence, and cognitive radio. In 2008, she joined the Green Radio Team, Imec, as a Principal Scientist. She is currently an Associate Professor with the Electrical Engineering Department, KU Leuven. Her current research interests include networked systems that require networks that are ever denser, heterogeneous, battery powered, and spectrum constrained.

Dr. Pollin is a BAEF and Marie Curie Fellow.